Original Article

Clara cell secretory protein 16 protects against PM2.5-induced ferroptosis in mouse lung epithelial cells in a concentration-dependent manner

Aili Wang¹, Jinle Lin², Shuo Yang¹

¹Pulmonary and Critical Care Medicine, Wuhan No. 1 Hospital, Wuhan 430022, Hubei, China; ²Department of Emergency Medicine, The Second Affiliated Hospital of Shenzhen University (People's Hospital of Shenzhen Baoan District), Shenzhen 518101, Guangdong, China

Received June 16, 2025; Accepted September 12, 2025; Epub October 15, 2025; Published October 30, 2025

Abstract: Background Clara cell secretory protein 16 (CC16) has been reported to exert anti-inflammatory and antioxidant effects. However, its underlying mechanism remains unclear. This study aimed to investigate the protective effect and mechanism of CC16 using an in vitro model of PM2.5-induced mouse pulmonary epithelial cells (TC-1), with a specific focus on its concentration-dependent effects. Methods: TC-1 cells were exposed to PM2.5 to induce inflammatory injury and ferroptosis, followed by treatment with CC16 at different concentrations (0.25, 0.5, and 1.0 µg/mL). TC-1 cells were divided into six groups: control, CC16, PM2.5, PM2.5 + CC16 (0.25 µg/mL), PM2.5 + CC16 (0.5 µg/mL), and PM2.5 + CC16 (1.0 µg/mL) groups. Cell viability was assessed using the Cell Counting Kit-8 assay. Levels of inflammatory cytokines (interleukin (IL)-5, IL-6, IL-13, IL-17A, and IL-1β) in the supernatant were measured by enzyme-linked immunosorbent assay. Protein expression levels of Nrf2, ACSL4, SLC7A11, and GPX4 were detected using western blotting. Intracellular reactive oxygen species (ROS) were detected with a fluorescent probe, and mitochondrial membrane potential (MMP) was measured by JC-1 staining. Glutathione (GSH), malondialdehyde (MDA), and Fe²⁺ content were measured using relevant kits. Mitochondrial ferroptosis features were observed by transmission electron microscopy (TEM). Results: PM2.5 exposure significantly reduced cell viability, aggravated inflammation, induced ferroptosis, and disrupted the integrity of mouse pulmonary epithelial cells. CC16 treatment reversed these effects in a concentration-dependent manner. Conclusions: CC16 effectively mitigates PM2.5-induced cellular injury in mouse pulmonary epithelial cells through inhibition of ferroptosis, with its protective effect showing a clear concentration dependence. These findings suggest CC16 as a novel strategy for PM2.5induced respiratory disease.

Keywords: CC16, ferroptosis, PM2.5, pulmonary epithelial cells

Introduction

Rapid industrial development has intensified air pollution, particularly the inhalation of particulate matter, posing a serious threat to the human respiratory system. Among these pollutants, PM2.5 - a major component of atmospheric fine particulate matter, is characterized by its aerodynamic diameter ($\leq 2.5~\mu m$), enabling it to penetrate the respiratory tract to reach the alveoli. PM2.5 induces oxidative stress, inflammatory responses, and other pathophysiologic processes. It ultimately leads to lung tissue injury and the development of respiratory diseases [1, 2]. Studies have shown that PM2.5 triggers ferroptosis in bronchial epithe-

lial cells by inducing iron metabolism disorders and redox homeostasis, with this novel form of cell death playing a crucial role in the mechanism of pulmonary toxicity [3, 4].

Nuclear factor erythroid 2-related factor 2 (Nrf2), a core regulator of the cellular antioxidant defense system, is essential for maintaining redox balance and regulating ferroptosis [5-8]. Nrf2 remains sequestered by Kelch-like ECH-associated protein 1 (Keap1) under resting conditions, but becomes activated upon exposure to oxidative and electrophilic stimuli [5, 9]. During oxidative stress, Nrf2 translocates to the nucleus and binds to antioxidant response elements, thereby inducing the transcription of

a series of antioxidant genes, including heme oxygenase-1 (HO-1) [9, 10], glutathione peroxidase 4 (GPX4) [11, 12], and solute carrier family 7 member 11 (SLC7A11) [12], which together establish an intrinsic protective mechanism. HO-1 catalyzes the degradation of heme into bilirubin, carbon monoxide, and iron ions, increasing intracellular antioxidant capacity and suppressing pro-inflammatory mediators [13]. GPX4 is the only enzyme capable of specifically clearing lipid peroxides, playing a critical role in inhibiting ferroptosis by catalyzing the reduction of lipid peroxides through glutathione (GSH), thus maintaining cell membrane stability [14]. SLC7A11, a critical component of the cystine/glutamate antiporter (system Xc⁻), facilitates cystine uptake, which is subsequently converted to cysteine for GSH synthesis, thus enhancing the cell's antioxidant capability [15]. The coordinated expression of these genes constitutes an effective self-protection response against damage caused by external stimuli.

Clara cell secretory protein 16 (CC16), a bioactive protein (molecular weight 16 kDa) secreted by Clara cells of the respiratory epithelium, exhibits anti-inflammatory and antioxidant properties in respiratory diseases. Recent clinical research has shown that CC16 expression is negatively correlated with the risk and severity of chronic airway inflammatory diseases, including chronic obstructive pulmonary disease and asthma [16, 17]. This suggests that higher CC16 levels are associated with a reduced disease incidence and milder conditions. The antiinflammatory effect of CC16 may involve inhibition of inflammatory cell activation and suppression of inflammatory factors [18]. However, its protective role and molecular mechanisms in PM2.5-induced airway epithelial injury remain incompletely understood. Systematic research on the potential of CC16 to modulate PM2.5-induced ferroptosis is scarce, and the role of the Nrf2 signaling pathway in its protective effects, as well as their concentration dependence, remain unknown.

In this study, we established a PM2.5-exposed mouse pulmonary epithelial cell model to investigate the cytoprotective effects of CC16 and its underlying mechanism. The results demonstrated that CC16 effectively inhibited PM2.5-induced ferroptosis through activation of the

Nrf2/GPX4 signaling pathway, with its protective effects showing a clear dose-response relationship.

Materials and methods

PM2.5 sample preparation

PM2.5 samples used in this study were provided by the Guangzhou Institute of Geochemistry, Chinese Academy of Sciences, collected between July and November 2019. The specific sampling procedure has been described previously [18]. Briefly, quartz fiber filter membranes (20×25 cm²) containing PM2.5 were cut into small pieces and immersed in 300 mL of ultrapure water, subjected to ultrasonic vibration, and centrifuged at 4°C and 9000 r/min for 1 h. The supernatant was discarded and the sediment was collected and freeze-dried at -80°C for 48 h to obtain PM2.5 powder, which was stored at -20°C for subsequent experiments.

Cell culture and treatment

TC-1 mouse lung epithelial cells were sub-cultured in RPMI-1640 complete medium (SH30-027, Hyclone) containing 10% fetal bovine serum (SH30084.03, Hyclone) and 1% penicillin-streptomycin (SV30010, Hyclone) under standard culture conditions (37°C, 5% CO_o). Initially, TC-1 cells at 90% confluence were seeded into 6-well plates at a density of 5×105 cells/well, allowed to adhere overnight in an incubator, and then exposed to 100 µg/mL PM2.5 (sterilized by autoclaving). The cells were divided into the following treatment groups: (1) phosphate-buffered saline (PBS) control; (2) CC16 (2 mg/kg; 50291-M08H-2mg, Sino Biological, China) at different concentrations (0.25, 0.5, and 1 μ g/mL); (3) PM2.5 exposure; and (4) PM2.5 + different concentrations of CC16. After 24 h of PM2.5 exposure, the medium was replaced with fresh medium containing the indicated concentration of CC16, and the cells were incubated for another 24 h.

Cell viability assay

Following treatment, cells from each group were seeded into 96-well plates at 5×10³ cells/mL and cultured overnight. Cell viability was measured using a Cell Counting Kit-8 (CCK-8)

assay (CK04, Dojindo, Japan) according to the manufacturer's instructions. Briefly, after washing twice with medium, 100 μ L RPMI-1640 medium and 10 μ L CCK solution were added to each well. The absorbance value at 450 nm was measured using a microplate reader (MULTISKAN MK3, Thermo, USA).

Enzyme-linked immunosorbent assay (ELISA)

Levels of the inflammatory cytokines, including interleukin (IL)-5 (E-EL-M0722c, Elabscience, China), IL-6 (EK206/3-96, Multi Sciences, China), IL-13 (70-EK213/2-96, Multi Sciences, China), IL-17A (E-EL-M0047c, Elabscience, China), and IL-1 β (E-EL-M0037c, Elabscience, China), in cell culture supernatants were quantified using ELISA kits, according to the respective manufacturer's instructions.

Malondialdehyde (MDA) and Glutathione (GSH) assays

After rinsing TC-1 cells with PBS, pellets were collected via low-speed centrifugation, resuspended in 0.3 mL isotonic PBS, and lysed by sonication. MDA (A003-1, Nanjing Jiancheng, China) and GSH (A006-2-1, Nanjing Jiancheng, China) levels were measured in 0.1 mL of cell suspension according to the corresponding kit protocols.

Reactive Oxygen Species (ROS) detection

Intracellular ROS levels were measured using a dichlorodihydrofluorescein diacetate (DCFH-DA) fluorescent probe (CA1410, Solarbio, China). Following treatment, cells were washed twice with serum-free RPMI-1640 medium, incubated with 10 μ M DCFH-DA solution (diluted in serum-free medium) at 37 °C for 20 min in the dark, trypsinized, centrifuged at 1000 rpm for 5 min, washed twice with PBS, and resuspended in 500 μ L PBS. Fluorescence intensity was analyzed by flow cytometry (Beckmann Kurtz, CytoFLEX S) at excitation/emission wavelengths of 488/525 nm. Three replicate wells were set per group, and ROS levels were expressed as mean fluorescence intensity.

Mitochondrial Membrane Potential (MMP) assay

MMP was assessed using a JC-1-based detection kit (M8650, Solarbio, China). Following

treatment, cells were incubated with 1 mL JC-1 working solution (1x) at 37°C for 20 min, washed twice with JC-1 buffer, and examined under a fluorescence microscope (Olympus IX73) to visualize red fluorescence (high MMP) and green fluorescence (low MMP). The red/green fluorescence ratio was also quantified by flow cytometry (excitation/emission: 585/590 nm for red; 510/527 nm for green).

Intracellular Fe²⁺ level detection

Fe²⁺ content was determined using an iron assay kit (E-BC-F101, Elabscience, China) following the manufacturer's instructions, and absorbance was measured at 575 nm using a fluorescence microplate reader.

Western blot

TC-1 cells were lysed to extract total protein, and protein concentrations were determined using a bicinchoninic acid assay. Equal amounts of protein (30 µg) were mixed with 5× loading buffer (4:1), denatured at 100°C for 10 min, cooled, and stored at -20°C. Samples and a protein ladder were separated onto sodium dodecyl sulfate-polyacrylamide gels by electrophoresis at 80 V until the dve front reached the resolving gel, followed by 120 V until completion. Proteins were transferred onto polyvinylidene difluoride membranes at 100 V for 90 min, blocked with 5% nonfat milk for 1 h, and incubated overnight at 4°C with the following primary antibodies: glyceraldehyde 3-phosphate dehydrogenase (GAPDH; abs132004, Absin, China; 1:2500), GPX4 (ab125066, Abcam, Cambridge, UK; 1:1000), Nrf2 (A0674, Abclonal, China; 1:1000), SLC7A11 (26864-1-AP. Proteintech. China: 1:1000), and ACSL4 (ab155282, Abcam, UK; 1:5000). After washing with TBST, membranes were incubated with horseradish peroxidase-conjugated secondary antibody (7074S, Cell Signaling Technology, Danvers, MA, USA; 1:10,000) for 2 h at room temperature. Protein bands were visualized using a ChemiDoc™ XRS+ system. The band intensities were quantified using ImageJ software with GAPDH as internal control.

Transmission Electron Microscopy (TEM)

Cells were fixed with TEM fixative at 4° C for 2-4 h, pelleted, encapsulated in 1% agarose, and rinsed three times with 0.1 M PBS (pH 7.4) for

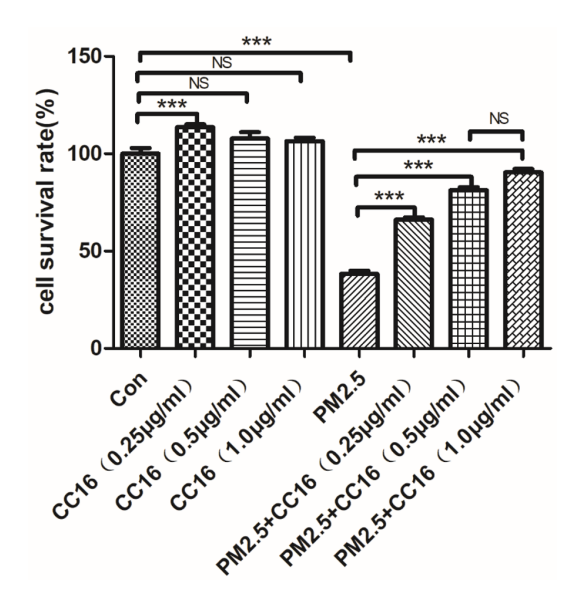


Figure 1. Effect of CC16 on the viability of mouse lung epithelial cells exposed to PM2.5. ***P < 0.001, ns P > 0.05. n=6, $\bar{x}\pm s$.

15 min each. Samples were post-fixed, dehydrated, infiltrated, embedded, sectioned into 60-80 nm slices, stained with uranyl acetate and lead citrate, dried overnight, and visualized using TEM (HT7700, Hitachi, Japan) for ultrastructural analysis.

Statistical analysis

Statistical analysis was performed using GraphPad Prism 8.0 (San Diego, CA, USA). Data were presented as mean \pm standard deviation. Multi-group comparisons were performed using one-way analysis of variance (ANOVA) followed by Tukey's *post hoc* test. Statistical significance was set at P \leq 0.05 (two-tailed).

Results

CC16 enhanced the viability of mouse lung epithelial cells

The effect of CC16 on the proliferation of mouse lung epithelial cells was assessed using the CCK-8 assay. Compared to the control group, cell viability was significantly increased in the CC16 (0.25 μ g/mL) group (P < 0.001), whereas no significant increases were observed at 0.5 μ g/mL or 1.0 μ g/(P > 0.05).

Cell viability was markedly reduced in the PM2.5-exposed group compared to the control group (P < 0.001). Treatment with CC16 (0.5 or 1.0 μ g/mL) significantly restored cell

viability compared to the PM2.5-exposed group alone, but the difference between the two (PM2.5+CC16 (0.5 ug/mL or 1.0 ug/mL)) groups was not significant (P > 0.05). No further increases in CC16 concentration were therefore tested in subsequent experiments (**Figure 1**).

CC16 attenuated PM2.5-induced inflammatory injury in mouse lung epithelial cells

To examine the anti-inflammatory effects of CC16, levels of IL-13, IL-6, IL-5, IL-1 β , and IL-17A were measured in cell supernatants by ELISA. Cytokine concentrations were significantly elevated in the PM2.5 group compared to the controls (P < 0.001). CC16 treatment markedly reduced the levels of these cytokines, with more pronounced decreases at higher CC16 concentrations (**Figure 2**).

CC16 inhibited lipid peroxidation in PM2.5-exposed mouse lung epithelial cells

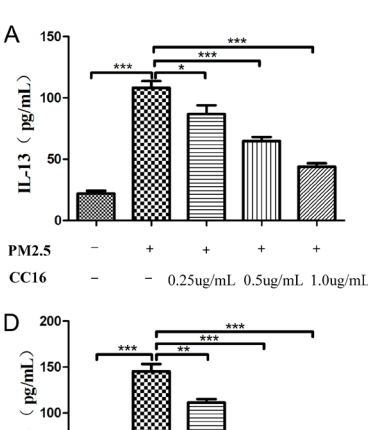
To investigate the antioxidative mechanism of CC16, intracellular GSH and MDA levels were quantified. PM2.5 exposure significantly decreased intracellular GSH levels and increased MDA levels compared to the control group (both P < 0.001). CC16 reversed these changes, causing more significant effects with increasing CC16 concentration (**Figure 3**).

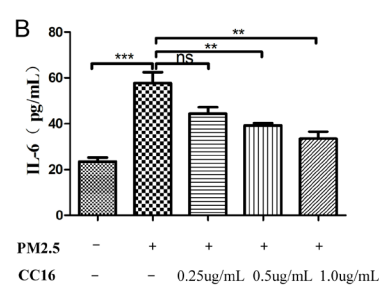
CC16 promoted the expression of Nrf2 and GPX4 in PM2.5-exposed mouse lung epithelial cells

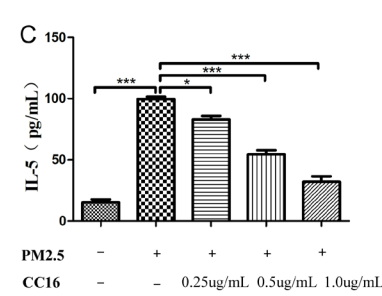
To clarify the protective mechanisms of CC16, the expression levels of the ferroptosis-related marker Nrf2 and its downstream factor GPX4 were examined by western blot. PM2.5 exposure significantly downregulated both Nrf2 and GPX4 protein levels compared to the control group (P < 0.01). CC16 treatment markedly increased expression levels of both proteins in PM2.5-exposed cells in a concentration-dependent manner (**Figure 4**).

CC16 inhibited mitochondrial ferroptosis in mouse lung epithelial cells

Mitochondrial morphology was assessed by TEM to further investigate the protective effects of CC16 on ferroptosis. Compared to the control group, PM2.5-exposed cells exhibited typical mitochondrial ferroptosis, characterized







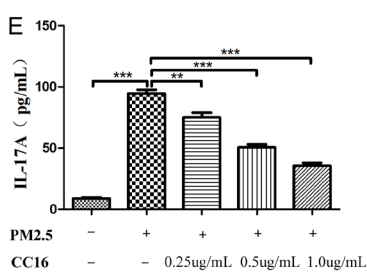
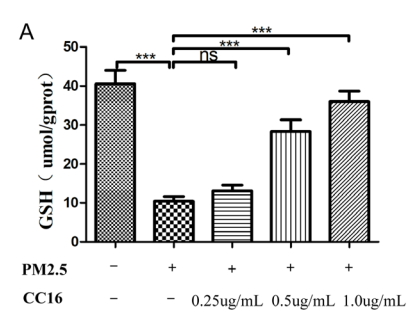


Figure 2. Effects of CC16 on inflammatory cytokine levels in the supernatant of mouse lung epithelial cells exposed to PM2.5. (A) interleukin (IL)-13; (B) IL-6; (C) IL-5; (D) IL-1 β ; and (E) IL-17A. *P < 0.05, **P < 0.01, ***P < 0.001, ns P > 0.05. n=6, $\overline{x}\pm s$.



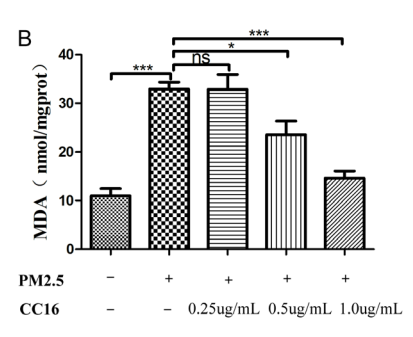


Figure 3. Effects of CC16 on glutathione (GSH) (A) and malondialdehyde (MDA) (B) levels in PM2.5-exposed mouse lung epithelial cells. *P < 0.05, ***P < 0.001, ns P > 0.05. n=6, $\overline{x}\pm s$.

by mitochondrial shrinkage, reduced size, increased outer-membrane density, elevated intramitochondrial electron density, iron deposition, and mitochondrial cristae swelling or reduction. CC16 alleviated these pathologic changes, with reduced mitochondrial shrinkage, lower membrane density, decreased iron deposition, and restoration of cristae structure, with greater effects at higher concentrations (Figure 5).

CC16 reduced intracellular ROS levels induced by PM2.5

ROS levels, assessed by fluorescence intensity, were significantly increased in PM2.5-exposed cells compared to controls (P < 0.001). ROS levels were significantly reduced in the PM2.5 + CC16 (0.25 $\mu g/mL)$ group compared with the PM2.5 group (P < 0.01), which were further decreased in the PM2.5 + CC16 (0.5 $\mu g/mL)$ and PM2.5 + CC16 (1.0 $\mu g/mL)$ groups in a

dose-dependent manner (P < 0.001, Figure 6).

CC16 maintained MMP in PM2.5-exposed cells

TEM and JC-1 staining revealed predominantly red fluorescence (high MMP) in mitochondria of the control group, whereas PM2.5 exposure led to a marked increase in green fluorescence (low MMP; P < 0.001). CC16 treatment

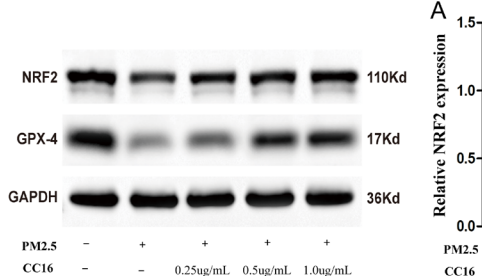
significantly increased the red fluorescence ratio in PM2.5-exposed cells in a dose-dependent manner, indicating a significant recovery of MMP in PM2.5+CC16 (1.0 ug/mL) group (P < 0.001, Figure 7).

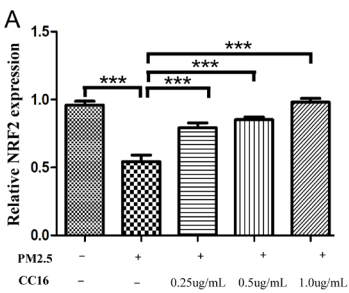
CC16 reduced intracellular Fe²⁺ accumulation in PM2.5-exposed cells

Colorimetric assays showed that intracellular Fe²⁺ content was significantly elevated in the PM2.5 group compared to controls (25.6 \pm 3.2 vs. 10.2 \pm 1.5 µg/mg protein, P < 0.001). Treatment with CC16 (1.0 µg/mL) markedly reduced Fe²⁺ content (15.8 \pm 2.1 µg/mg protein) compared to the PM2.5 group (P < 0.01, **Figure 8**).

CC16 regulated the expression of the ferroptosis-related molecules SLC7A11 and ACSL4

Western blot analysis revealed that SLC7A11 expression was significantly downregulated





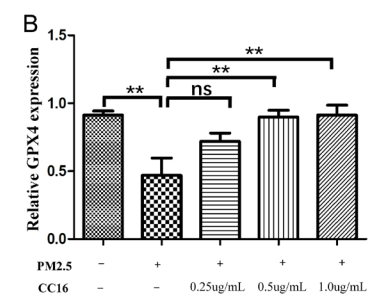


Figure 4. Effects of CC16 on Nrf2 (A) and GPX4 (B) protein expression in PM2.5-exposed mouse lung epithelial cells. **P < 0.01, ***P < 0.001, ns P > 0.05. n=6, $\bar{x}\pm s$.

(P < 0.001), whereas ACSL4 expression was significantly upregulated (P < 0.001) in the PM2.5 group compared to the control group. CC16 administration progressively increased SLC7A11 levels and decreased ACSL4 levels compared to the PM2.5 group. When the CC16 intervention concentration was 1.0 ug/ml, demonstrating the best effect (both P < 0.01, Figure 9).

Discussion

CC16, encoded by the SCGB1A1 gene located on chromosome 11q12.3, is a secretory protein primarily produced by airway Clara cells. It exerts multiple protective functions in the respiratory system, including inhibiting inflammatory cascades, regulating immune responses, and scavenging ROS [19-21]. Our previous work demonstrated that recombinant CC16 significantly inhibited LPS-induced apoptosis in A549 alveolar epithelial cells, promoted cell proliferation, and reduced pro-inflammatory cytokine release [22], closely associated with its anti-oxidative capacity. CC16 also alleviated airway inflammation by inhibiting airway epithelial pyroptosis in a PM2.5-induced asthma mouse model [23]. Moreover, extracellular vesicle-derived CC16 suppressed inflammation and DNA damage responses by downregulating NF-kB signaling, suggesting its potential as a therapeutic candidate for acute lung injury [24]. Recombinant CC16 has also been shown to mitigate inflammation, oxidative stress, apoptosis, and autophagy by inhibiting the p38MAPK pathway in neonatal rat sepsis [25]. Despite these advances, the concentrationdependent effects and underlying mechanisms by which CC16 counteracts PM2.5-induced ferroptotic injury in lung epithelial cells, particularly for complex air pollutants such as PM2.5, however, remain unclear.

Lung epithelial cells serve as the first line of defense against inhaled pollutant particles. PM2.5 exposure can induce airway epithelial inflammation, increase permeability, and trigger ferroptosis [18, 26, 27]. Consistent with previous studies, our findings demonstrated that PM2.5 exposure induced hallmark features of ferroptosis in mouse lung epithelial cells, including mitochondrial shrinkage, cristae fragmentation, and abnormal iron ion deposition in the matrix (manifested as increased particle density) observed by TEM. We also detected significant reductions in GSH, elevations in MDA levels, enhanced ACSL4 expression, and increased secretion of inflammatory cytokines in the culture supernatants. This further confirmed ferroptosis as a critical pathologic component of PM2.5-induced lung toxicity.

To further elucidate the mechanisms and concentration-dependent effects of CC16, we assessed intracellular Fe2+ levels, mitochondrial morphology (TEM), MMP (JC-1 staining), ferroptosis-related proteins (Nrf2, GPX4, SLC7A11, and ACSL4), oxidative stress markers (MDA, ROS, and GSH), and inflammatory cytokine release. Notably, CC16 restored mitochondrial architecture, reduced iron particle deposition. and reestablished redox homeostasis. In addition, GSH levels were significantly increased, while MDA, ROS content, and ACSL4 expression were decreased. Moreover, CC16 upregulated Nrf2 and its downstream targets GPX4 and SLC7A11. Levels of inflammatory cytokines (IL-13, IL-6, IL-5, IL-1β, IL-17A) in the cell culture supernatant were also significantly reduced, with more pronounced reduction at higher CC16 concentrations.

Ferroptosis, a novel, iron-dependent form of programmed cell death, is closely associated

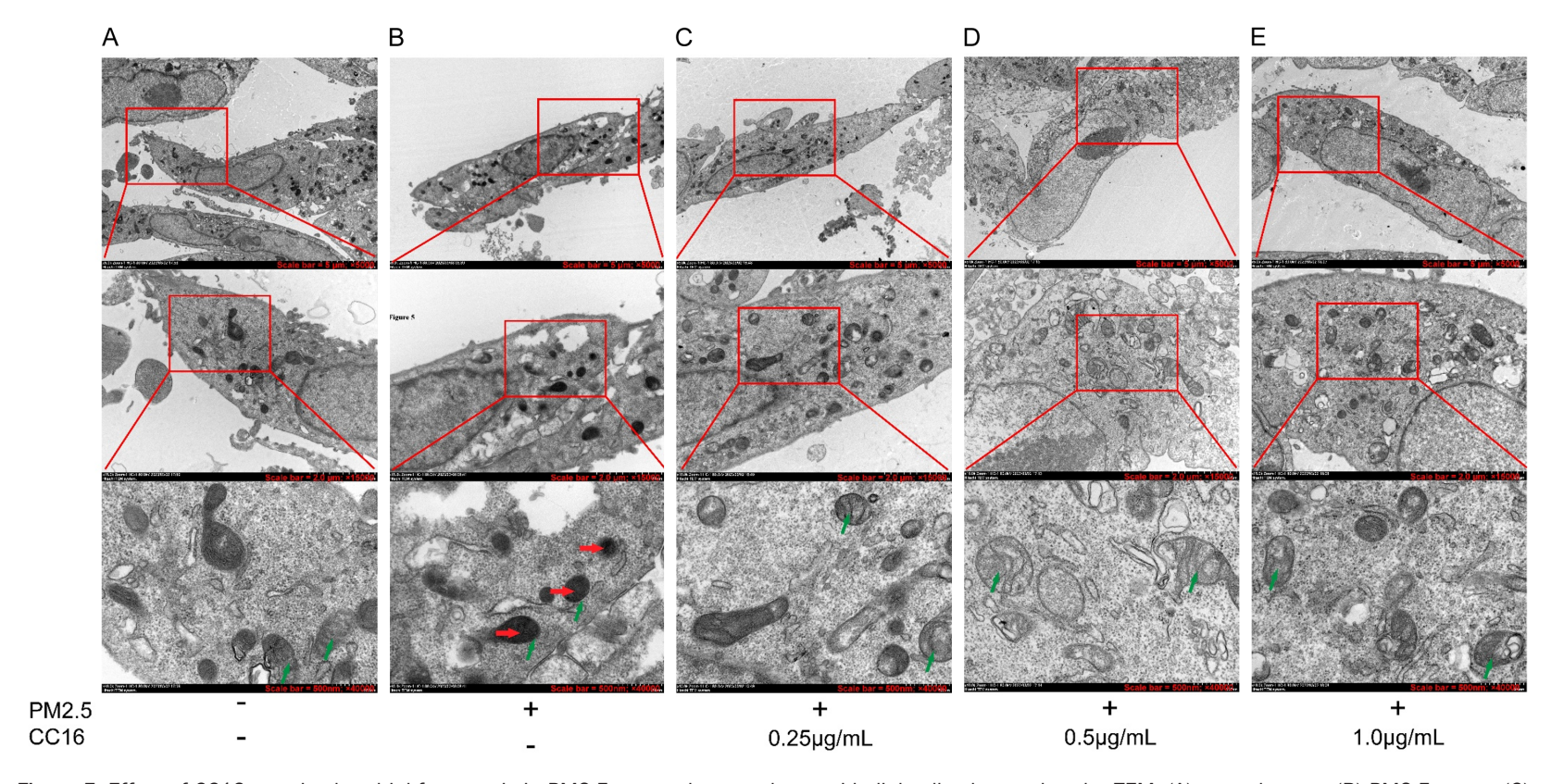


Figure 5. Effect of CC16 on mitochondrial ferroptosis in PM2.5-exposed mouse lung epithelial cells observed under TEM. (A) control group, (B) PM2.5 group, (C) PM2.5 + CC16 (0.25 μ g/mL) group, (D) PM2.5 + CC16 (0.5 μ g/mL) group, and (E) PM2.5 + CC16 (1.0 μ g/mL) group. Green arrows indicate mitochondria; red arrows indicate iron deposition, reduced or absent cristae, and mitochondrial shrinkage.

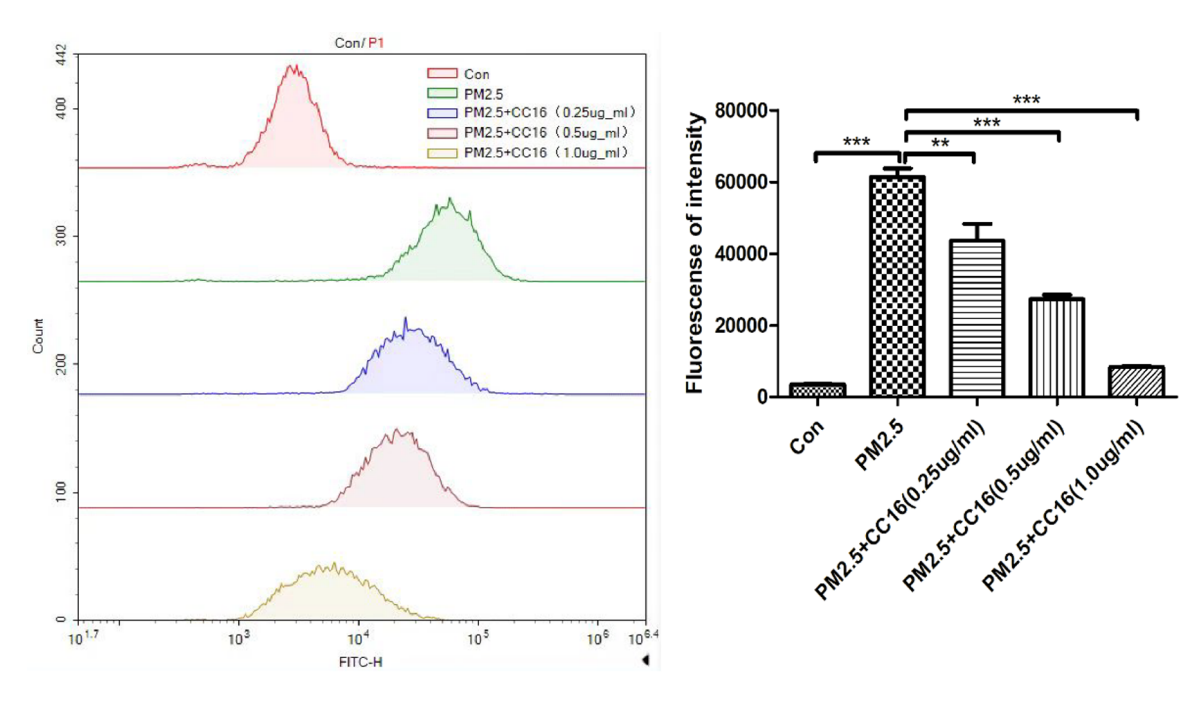
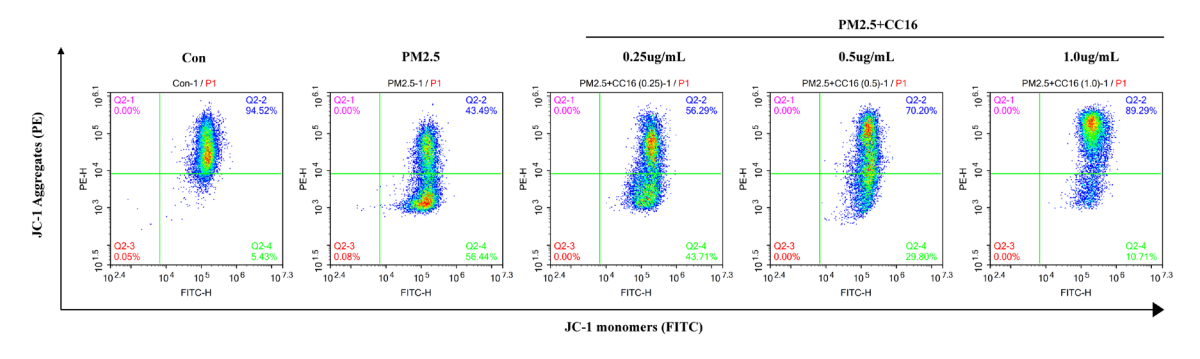


Figure 6. Effect of CC16 on reactive oxygen species (ROS) levels in PM2.5-exposed mouse lung epithelial cells. Histogram of ROS fluorescence intensity measured by flow cytometry. **P < 0.01, ***P < 0.001. n=6, $\bar{x} \pm s$.



Membrane potential

Figure 7. Effect of CC16 on mitochondrial membrane potential (MMP) in PM2.5-exposed mouse lung epithelial cells. Red/green fluorescence ratio measured by flow cytometry. *P < 0.05, ***P < 0.001, ns: P > 0.05. n=6, $\bar{x} \pm s$.

with lipid peroxidation and iron metabolism dysregulation [28]. Lipid peroxidation produces lipid peroxides and MDA, both of which accumulate during ferroptosis, leading to GSH depletion [29, 30]. Nrf2, a core regulator of the cellular antioxidant defense system, plays a pivotal role in antioxidation. Under stress conditions, Nrf2 translocates into the nucleus,

binds directly to antioxidant response elements in gene promoters, and activates downstream antioxidant genes, including GPX4, thereby constituting a major defense against ferroptosis [31]. GPX4, a selenium-dependent glutathione peroxidase, uniquely reduces hydrogen peroxide in membrane lipids and represents a cornerstone of the anti-peroxidative defense sys-

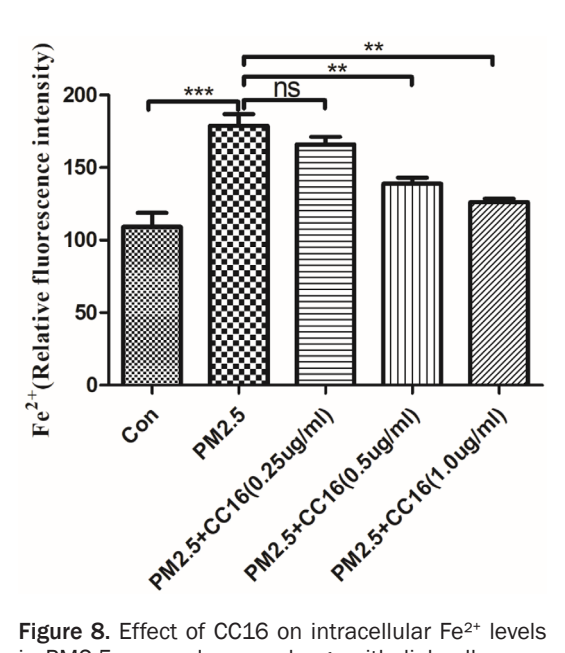


Figure 8. Effect of CC16 on intracellular Fe²⁺ levels in PM2.5-exposed mouse lung epithelial cells measured by colorimetric assay. **P < 0.01, ***P < 0.001, ns: P > 0.05. n=6, $\bar{x}\pm s$.

tem [32]. The Nrf2/GPX4 signaling pathway has been implicated in ferroptosis across multiple disease processes [33, 34]. Our results showed that PM2.5 exposure significantly suppressed the Nrf2/GPX4 axis, whereas CC16 treatment activated this pathway in a dosedependent manner. Given its anti-oxidative and anti-inflammatory properties, CC16 may protect against PM2.5-induced ferroptosis by scavenging ROS, reducing Nrf2 protein degradation, enhancing Keap1-Nrf2 dissociation, promoting Nrf2 nuclear translocation, upregulating GPX4 expression, and enhancing cellular detoxification of lipid peroxidation products.

CC16 also demonstrated a unique bidirectional regulatory effect on key ferroptosis modulators. It significantly upregulated SLC7A11 expression, a target of activated Nrf2 that regulates the the GSH/GPX4 axis, as the principal pathway for ferroptosis inhibition [4], while concurrently downregulating ACSL4 expression. The latter effect activates diverse polyunsaturated fatty acids, remodels cellular lipid composition, and increases cellular susceptibility to ferroptosis [35]. This dual-target mechanism highlights the ability of CC16 to inhibit ferroptosis by simultaneously bolstering the antioxidant defense (through the SLC7A11/GSH axis) and reducing pro-ferroptotic lipid metabolism (through ACSL4 suppression).

Activation of the Nrf2/GPX4 pathway by CC16 appears essential for maintaining mitochondrial integrity, as the organelle most vulnerable during ferroptosis [36]. In this study, PM2.5 exposure induced severe mitochondrial damage, including matrix condensation, cristae fragmentation, and mitochondrial shrinkage, as hallmark morphologic features of ferroptosis. Crucially, CC16 treatment not only prevented MMP depolarization but also reversed structural damage, thereby preserving mitochondrial function and suppressing ferroptotic progression. Mechanistically, this protection is closely associated with activation of the Nrf2/GPX4 axis, and our preliminary data showed that CC16 promoted Nrf2 nuclear translocation. Mechanistically, GPX4, upregulated downstream of Nrf2, plays a pivotal role in detoxifying mitochondrial membrane lipid peroxides, directly protecting mitochondrial structure by reducing phospholipid hydroperoxides. Collectively, these findings indicate that CC16, through concentration-dependent activation of the Nrf2/GPX4 pathway, provides organelle-level protection against ferroptosis and represents a novel paradigm for targeting mitochondrial injury.

In summary, our findings suggest that CC16 alleviates PM2.5-induced cytotoxic injury in mouse lung epithelial cells by inhibiting ferroptosis by the Nrf2/GPX4 pathway in a concentration-dependent manner, providing a new theoretical basis for the prevention and treatment of PM2.5-related lung diseases. This study delineated the critical role of the Nrf2/ GPX4 pathway in mediating the anti-ferroptotic effects of CC16; however, the precise upstream mechanisms by which CC16 activates Nrf2 signaling and regulates iron metabolism-related genes (e.g., FTH1, TFR1) remain to be clarified. Moreover, as these findings were derived from in vitro experiments, further in vivo studies are needed to confirm these findings. Future studies should also identify the specific receptors mediating CC16 activity and clarify its direct effect on iron regulatory networks.

Acknowledgements

We thank Susan Furness, PhD, from Liwen Bianji (Edanz) (www.liwenbianji.cn) for editing the English text of a draft of this manuscript. This research was supported by the Hubei

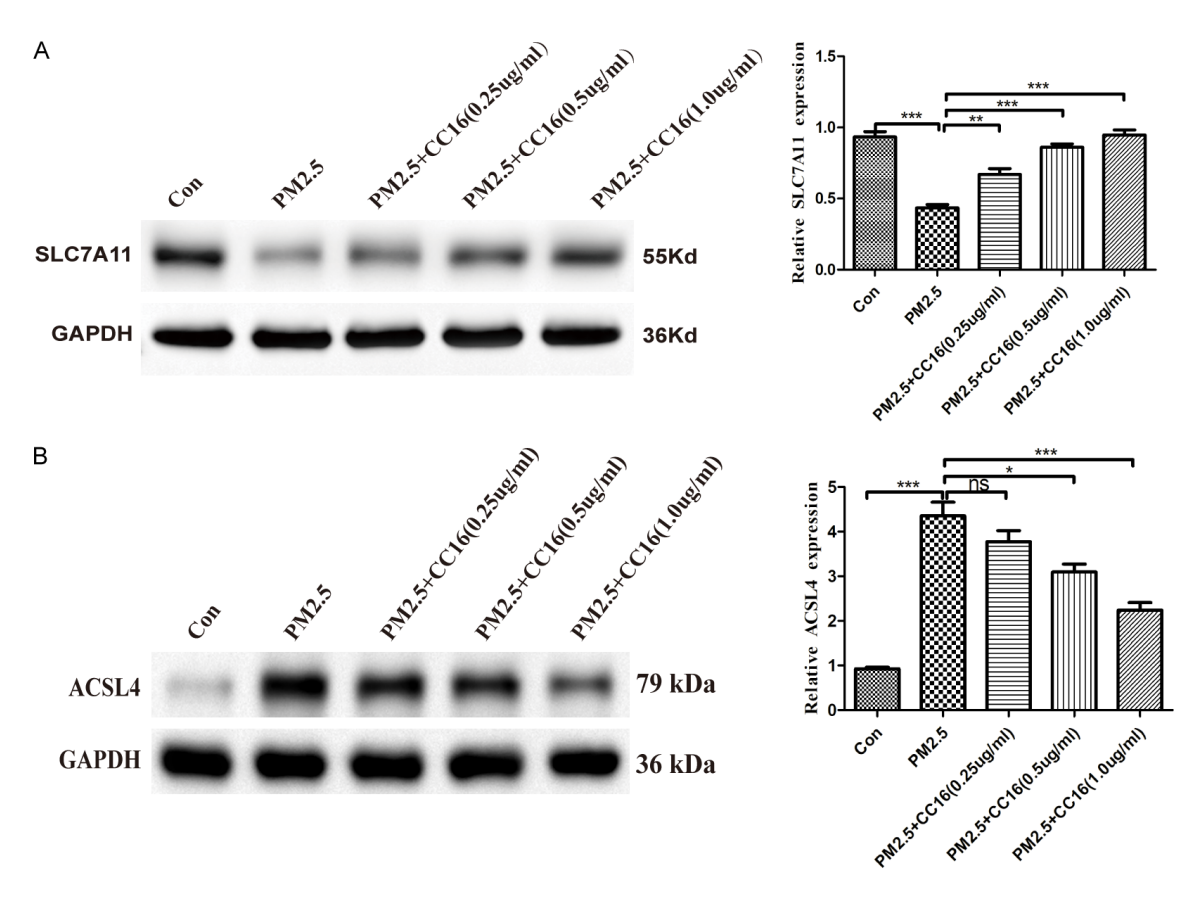


Figure 9. Effects of CC16 on SLC7A11 (A) and ACSL4 (B) protein expression in PM2.5-exposed mouse lung epithelial cells. **P < 0.01, ***P < 0.001, ns: P > 0.05. n=6, \overline{x} ±s.

Provincial Natural Science Foundation (Grant No. 2024AFB1032), and the Hubei Provincial Public Health Youth Top-notch Talent Training Program, the National Natural Science Fund of China (No. 82302462), the Guang Dong Basic and Applied Basic Research Foundation (No. 2022A1515111206), the Science and Technology Planning Project of Shenzen Municipality (No. YJ20230807140904010).

Disclosure of conflict of interest

None.

Address correspondence to: Dr. Shuo Yang, Pulmonary and Critical Care Medicine, Wuhan No. 1 Hospital, Wuhan 430022, Hubei, China. Tel: +86-027-85805974; E-mail: m13871032441@163.com

References

[1] Deng Q, Deng L, Miao Y, Guo X and Li Y. Particle deposition in the human lung: health implications of particulate matter from different sources. Environ Res 2019; 169: 237-245.

- [2] Shi J, Chen R, Yang C, Lin Z, Cai J, Xia Y, Wang C, Li H, Johnson N, Xu X, Zhao Z and Kan H. Association between fine particulate matter chemical constituents and airway inflammation: a panel study among healthy adults in China. Environ Res 2016; 150: 264-268.
- [3] Zhang Y, Jiang M, Xiong Y, Zhang L, Xiong A, Wang J, He X and Li G. Integrated analysis of ATAC-seq and RNA-seq unveils the role of ferroptosis in PM2.5-induced asthma exacerbation. Int Immunopharmacol 2023; 125: 111209.
- [4] Wang X, Wang Y, Huang D, Shi S, Pei C, Wu Y, Shen Z, Wang F and Wang Z. Astragaloside IV regulates the ferroptosis signaling pathway via the Nrf2/SLC7A11/GPX4 axis to inhibit PM2.5-mediated lung injury in mice. Int Immunopharmacol 2022; 112: 109186.
- [5] Baird L and Yamamoto M. The molecular mechanisms regulating the KEAP1-NRF2 pathway. Mol Cell Biol 2020; 40: e00099-20.
- [6] O'Rourke SA, Shanley LC and Dunne A. The Nrf2-HO-1 system and inflammaging. Front Immunol 2024; 15: 1457010.
- Yang Y, Han J, Wei Y, Jin J and Feng W. Research progress on ferroptosis in Myelodysplas-

- tic syndromes. Front Pharmacol 2025; 16: 1561072.
- [8] She W, Su J, Ma W, Ma G, Li J, Zhang H, Qiu C and Li X. Natural products protect against spinal cord injury by inhibiting ferroptosis: a literature review. Front Pharmacol 2025; 16: 1557133.
- [9] Li J, Lu K, Sun F, Tan S, Zhang X, Sheng W, Hao W, Liu M, Lv W and Han W. Panaxydol attenuates ferroptosis against LPS-induced acute lung injury in mice by Keap1-Nrf2/H0-1 pathway. J Transl Med 2021; 19: 96.
- [10] Chen Y, Wang J, Li J, Zhu J, Wang R, Xi Q, Wu H, Shi T and Chen W. Astragalus polysaccharide prevents ferroptosis in a murine model of experimental colitis and human Caco-2 cells via inhibiting NRF2/H0-1 pathway. Eur J Pharmacol 2021; 911: 174518.
- [11] Zhang Z, Fu C, Liu J, Sai X, Qin C, Di T, Yang Y, Wu Y and Bian T. Hypermethylation of the Nrf2 promoter induces ferroptosis by inhibiting the Nrf2-GPX4 axis in COPD. Int J Chron Obstruct Pulmon Dis 2021; 16: 3347-3362.
- [12] Deng X, Lin B, Wang F, Xu P and Wang N. Mangiferin attenuates osteoporosis by inhibiting osteoblastic ferroptosis through Keap1/ Nrf2/SLC7A11/GPX4 pathway. Phytomedicine 2024; 124: 155282.
- [13] Che J, Yang J, Zhao B and Shang P. HO-1: a new potential therapeutic target to combat osteoporosis. Eur J Pharmacol 2021; 906: 174219.
- [14] Huang B, Wang H, Liu S, Hao M, Luo D, Zhou Y, Huang Y, Nian Y, Zhang L, Chu B and Yin C. Palmitoylation-dependent regulation of GPX4 suppresses ferroptosis. Nat Commun 2025; 16: 867.
- [15] Li P, Yu J, Huang F, Zhu YY, Chen DD, Zhang ZX, Xie ZC, Liu ZY, Hou Q, Xie N, Peng TH, Chen X, Li L and Xie W. SLC7A11-associated ferroptosis in acute injury diseases: mechanisms and strategies. Eur Rev Med Pharmacol Sci 2023; 27: 4386-4398.
- [16] Gribben KC, Poole JA, Nelson AJ, Farazi PA, Wichman CS, Heires AJ, Romberger DJ and LeVan TD. Relationships of serum CC16 levels with smoking status and lung function in COPD. Respir Res 2022; 23: 247.
- [17] Li X, Guerra S, Ledford JG, Kraft M, Li H, Hastie AT, Castro M, Denlinger LC, Erzurum SC, Fahy JV, Gaston B, Israel E, Jarjour NN, Levy BD, Mauger DT, Moore WC, Zein J, Kaminski N, Wenzel SE, Woodruff PG, Meyers DA and Bleecker ER. Low CC16 mRNA expression levels in bronchial epithelial cells are associated with asthma severity. Am J Respir Crit Care Med 2023; 207: 438-451.
- [18] Wang A, Liu J, Li Z, Qian Z, Yang S, Luo S, Lin J and Wu J. CC16 alleviates PM2.5-induced lung epithelial cell injury and airway inflammation in

- asthmatic mice by inhibiting ferroptosis. Ecotoxicol Environ Saf 2025; 289: 117417.
- [19] Janicova A, Becker N, Xu B, Wutzler S, Vollrath JT, Hildebrand F, Ehnert S, Marzi I, Stormann P and Relja B. Endogenous uteroglobin as intrinsic anti-inflammatory signal modulates monocyte and macrophage subsets distribution upon sepsis induced lung injury. Front Immunol 2019; 10: 2276.
- [20] Kurowski M, Jurczyk J, Jarzebska M, Moskwa S, Makowska JS, Krysztofiak H and Kowalski ML. Association of serum Clara cell protein CC16 with respiratory infections and immune response to respiratory pathogens in elite athletes. Respir Res 2014; 15: 45.
- [21] Almuntashiri S, Han Y, Zhu Y, Dutta S, Niazi S, Wang X, Siddiqui B and Zhang D. CC16 regulates inflammation, ROS generation and apoptosis in bronchial epithelial cells during klebsiella pneumoniae infection. Int J Mol Sci 2021; 22: 11459.
- [22] Lin J, Li J, Shu M, Wu W, Zhang W, Dou Q, Wu J and Zeng X. The rCC16 protein protects against LPS-induced cell apoptosis and inflammatory responses in human lung pneumocytes. Front Pharmacol 2020; 11: 1060.
- [23] Lin J, Chen X, Chen Y, Zeng X, Wang F, Luo S, Jiang L, Hu W, Liu X, Zhang J and Wu J. Club cell secretory protein 16 promotes cell proliferation and inhibits inflammation and pyroptosis in response to particulate matter 2.5-induced epithelial damage in asthmatic mice. J Thorac Dis 2025; 17: 753-773.
- [24] Han Y, Zhu Y, Almuntashiri S, Wang X, Somanath PR, Owen CA and Zhang D. Extracellular vesicle-encapsulated CC16 as novel nanotherapeutics for treatment of acute lung injury. Mol Ther 2023; 31: 1346-1364.
- [25] Zhou R, Qu Y, Huang Q, Sun X, Mu D and Li X. Recombinant CC16 regulates inflammation, oxidative stress, apoptosis and autophagy via the inhibition of the p38MAPK signaling pathway in the brain of neonatal rats with sepsis. Brain Res 2019; 1725: 146473.
- [26] Liu X, Li Z, Shan J, Wang F, Li Z, Luo S and Wu J. PM(2.5) exposure inhibits transepithelial anion short-circuit current by downregulating P2Y2 receptor/CFTR pathway. Int J Med Sci 2024; 21: 1929-1944.
- [27] Guohua F, Tieyuan Z, Xinping M and Juan X. Melatonin protects against PM2.5-induced lung injury by inhibiting ferroptosis of lung epithelial cells in a Nrf2-dependent manner. Ecotoxicol Environ Saf 2021; 223: 112588.
- [28] Jiang X, Stockwell BR and Conrad M. Ferroptosis: mechanisms, biology and role in disease. Nat Rev Mol Cell Biol 2021; 22: 266-282.

- [29] Wenzel SE, Tyurina YY, Zhao J, St Croix CM, Dar HH, Mao G, Tyurin VA, Anthonymuthu TS, Kapralov AA, Amoscato AA, Mikulska-Ruminska K, Shrivastava IH, Kenny EM, Yang Q, Rosenbaum JC, Sparvero LJ, Emlet DR, Wen X, Minami Y, Qu F, Watkins SC, Holman TR, VanDemark AP, Kellum JA, Bahar I, Bayir H and Kagan VE. PEBP1 wardens ferroptosis by enabling lipoxygenase generation of lipid death signals. Cell 2017; 171: 628-641, e626.
- [30] Tang D, Chen X, Kang R and Kroemer G. Ferroptosis: molecular mechanisms and health implications. Cell Res 2021; 31: 107-125.
- [31] Jiang X, Yu M, Wang WK, Zhu LY, Wang X, Jin HC and Feng LF. The regulation and function of Nrf2 signaling in ferroptosis-activated cancer therapy. Acta Pharmacol Sin 2024; 45: 2229-2240.
- [32] Liu Y, Wan Y, Jiang Y, Zhang L and Cheng W. GPX4: the hub of lipid oxidation, ferroptosis, disease and treatment. Biochim Biophys Acta Rev Cancer 2023; 1878: 188890.

- [33] Chen H, Qian Y, Jiang C, Tang L, Yu J, Zhang L, Dai Y and Jiang G. Butyrate ameliorated ferroptosis in ulcerative colitis through modulating Nrf2/GPX4 signal pathway and improving intestinal barrier. Biochim Biophys Acta Mol Basis Dis 2024; 1870: 166984.
- [34] Du L, Guo C, Zeng S, Yu K, Liu M and Li Y. Sirt6 overexpression relieves ferroptosis and delays the progression of diabetic nephropathy via Nrf2/GPX4 pathway. Ren Fail 2024; 46: 2377785.
- [35] Jia B, Li J, Song Y and Luo C. ACSL4-mediated ferroptosis and its potential role in central nervous system diseases and injuries. Int J Mol Sci 2023; 24: 10021.
- [36] Yang R, Gao W, Wang Z, Jian H, Peng L, Yu X, Xue P, Peng W, Li K and Zeng P. Polyphyllin I induced ferroptosis to suppress the progression of hepatocellular carcinoma through activation of the mitochondrial dysfunction via Nrf2/HO-1/GPX4 axis. Phytomedicine 2024; 122: 155135.